

Recent Advances in Dynamic Identification and Response Simulation of Hybrid Base Isolation Systems



Athanasios A. Markou

*Department of Civil Engineering, Aristotle University, Thessaloniki, GR-54124, Greece,
e-mail: athanasiosmarkou@gmail.com*

Anastasia Athanasiou & Giuseppe Oliveto

*Department of Civil and Environmental Engineering, University of Catania, 95125, Italy,
e-mail: athanasiou@dica.unict.it & goliveto@dica.unict.it*

SUMMARY:

A physical model composed of a tri-linear spring, a friction slider and a viscous damper is proposed for the simulation of the dynamic behaviour of hybrid base isolation systems (HBIS) composed of high damping rubber bearings (HDRB) and low friction sliding bearings (LFSB). After the introduction of the constitutive equations for each device composing the overall system, it is shown that the motion of the system consists of alternating linear phases. An analytical solution is provided in compact form for all possible phases of motion. The end conditions for one phase provide the initial conditions for the next one. The solution is applied to the dynamic identification of the HBIS of the Solarino buildings. A well established evolution strategy (CMA-ES) is used as the dynamic identification algorithm. The estimated values of the physical parameters, together with simulated test responses, contribute to a better understanding of the behaviour of HBIS.

Keywords: Seismic Isolation; Dynamic Identification; Analytical Solution; Evolution Strategies.

1. INTRODUCTION

Hybrid Base Isolation Systems (HBIS), composed of High Damping Rubber Bearings (HDRB) and Low Friction Sliding Bearings (LFSB), are considered. At the turn of the century such systems were used for the seismic retrofitting of two four-story reinforced concrete buildings in Eastern Sicily, (Oliveto et al., 2004(a)). In July 2004 one of the buildings was subjected to free vibration tests by releasing imposed initial displacements, (Oliveto et al., 2004(b)).

In the following years most of the work by the senior author has been devoted to the identification of the base isolation system, using very simple models at first and moving gradually to more sophisticated ones. The work has been presented at conferences on earthquake engineering and published in reviewed journals. Identification in the frequency domain, (Oliveto et al., 2008), was followed by identification in the time domain (Oliveto et al., 2010). The latter involved a bi-linear model to describe the HDRB component of the system and a Constant Coulomb Friction Model (CCFM) for the LFSB component.

The identification was based on the Least Squares Method (LSM), used to match the experimental acceleration response to the analytical solution based on the above models. The results obtained were good and the identified parameters compared well with those derived from laboratory tests performed on individual bearings. Nevertheless, the work continued with the aim of improving both the model and the identification procedure: on one side by providing improved subsystem models and on the other by searching for the most effective algorithm for the problem at hand.

As far as the model is concerned, a Linear Coulomb Friction Model (LCFM) was introduced to exploit some characteristics of the experimental acceleration signal. The results of this study were presented at CUEE-2011 and were based again on an analytical solution. Apart from yielding improved identification results, this work also provided a simple way of evaluating the relative dissipation

capacity of the two system components, (Athanasίου and Oliveto, 2011).

From a computational point of view an interdisciplinary approach was used. A whole family of evolutionary algorithms (Evolution Strategies) were tested on the identification problem at hand and the most suitable one was identified, (Athanasίου et al., 2011 and 2012).

Object of the present paper is to summarize the previous work and to present the latest results based on newly developed models and a state-of-the-art identification algorithm. The new models include a tri-linear spring for the description of the behaviour of the HDRB component and a LCFM for the description of the behaviour of the LFSB component. The response is once more based on an analytical solution. The Covariance Matrix Adaptation-Evolution Strategy (CMA-ES), (Hansen, 2006), is used for the identification of the considered base isolation system. The results are compared to those obtained by use of the previous models and the characteristics of each model are analysed and discussed.

2. BASIC PRINCIPLE OF SEISMIC ISOLATION

Seismic isolation is based on the idea of decoupling the motion of the structure from the motion of the ground. Ideally a structure would be perfectly isolated from the horizontal seismic action if it could remain still while the ground slid freely underneath. Apart from the technological difficulty of implementing such idea, some practical points are also against the use of this ideal solution. Under horizontal forces, such as those due to wind, the structure would move without bounds and even under earthquakes there would be the danger of it colliding against obstacles fixed to the ground. To avoid these inconveniences the structure should have sufficient horizontal stiffness to sustain the horizontal forces and to limit the horizontal displacement relative to the ground to an acceptable level. This task can be achieved by using special bearings with low horizontal stiffness. A state-of-the-art of the general hardware used for seismic isolation can be found in a recent MCEER report, (Constantinou et al., 2007). Several recent constructions using seismic isolation in Japan are shown in a special issue of the Journal of Disaster Research, (Kasai, 2009), while several topics concerning seismic isolation and seismic isolation devices are addressed in a special issue of Earthquake Engineering and Structural Dynamics, (Wada and Constantinou, 2010).

A HBIS composed of 12 HDRB and 13 LFSB was designed and used for the Solarino buildings (Oliveto et al., 2004(a) and (b)). To avoid instability problems, the horizontal stiffness of each HDRB cannot be below certain limits and for this reason only 12 of the 25 bearings in the Solarino buildings are HDRB while the remaining 13 are LFSB. The latter are not exposed to instability problems and do not exhibit horizontal stiffness while sliding.

3. THE PHYSICAL MODEL

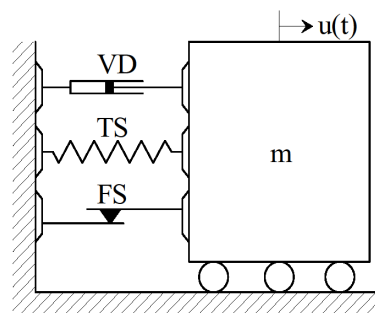


Figure 3.1. Single degree of freedom system

The physical model is the same as the one considered in (Oliveto et al., 2010). As shown in Fig. 3.1, it is composed of a mass m restrained by a non-linear spring, a viscous damper and a friction slider acting in parallel. The mass represents the part of the structure above the isolation interface assumed as rigid. This assumption is reasonable for low rise buildings, especially when the focus is on the isolation system, and is widely justified in the literature, (Oliveto et al., 2010) and referred literature. The non-linear spring is used to model the behaviour of the HDRB component of the isolation system while the friction slider describes the response of the LFSB. The viscous damper is meant to account for any source of energy dissipation in addition to the other two devices. For instance it could account for the energy dissipated in the superstructure.

4. MATHEMATICAL MODELS

Based on its purpose, a linear model is adopted for the viscous damper. This model has been used in all previous studies and is maintained in the present one. As far as the non-linear spring is concerned a bi-linear model was used in (Oliveto et al., 2010) and in (Athanasίου and Oliveto, 2011). In an attempt to improve previous identification results, herein the bi-linear spring is replaced by a tri-linear one, Fig. 4.1(a). It may be interesting to notice that the bi-linear model is a particular case of the tri-linear one when the yielding branches 2 and 3 have the same slope, i.e. $k_1=k_2$.

The friction slider was modelled by a CCFM in (Oliveto et al., 2010) and by a LCFM, with the amplitude of the friction force increasing with the amplitude of the displacement, in (Athanasίου and Oliveto, 2011). The use of the latter was motivated by the observation that when the velocity changes sign the acceleration records show larger jumps at higher amplitudes of the displacement. In the present work we are allowing for the friction force to diminish with the amplitude of the displacement, considering that the change of sign of the velocity occurs when the amplitude of the displacement is a maximum, but then the velocity is nearly zero and the friction force at a minimum. The proposed model is shown Fig. 4.1(b). It may be worth noticing that by setting $k_f=0$ in this model the CCFM used in (Oliveto et al., 2010) is regained, while by changing the sign to k_f the LCFM used in (Athanasίου and Oliveto, 2011) is found.

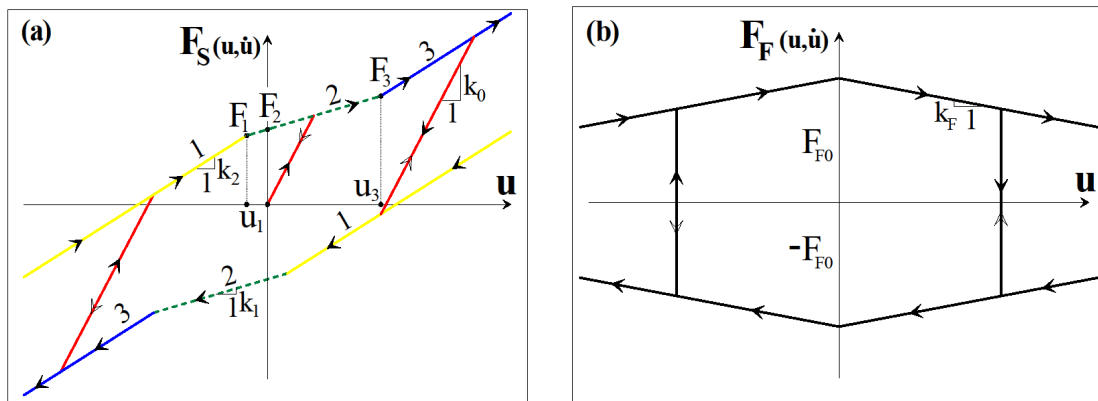


Figure 4.1. (a) Tri-linear model and (b) Linear Coulomb friction model

5. EQUATION OF MOTION

The equation of motion for the free vibration of the system shown in Fig. 3.1 can be written as follows:

$$m\ddot{u} + c\dot{u} + F_S(u, \dot{u}) + F_F(u, \dot{u}) = 0 \quad (5.1)$$

where $F_S(u, \dot{u})$ is the force in the tri-linear spring and $F_F(u, \dot{u})$ is the force in the friction slider.

5.1. Constitutive equations for the tri-linear model

The force in the tri-linear spring is graphically shown in Fig. 4.1(a) while the force in the friction slider is shown in Fig. 4.1(b). From observation of Fig. 4.1(a) it may be recognized that there are seven distinct phases of motion, e.g. six plastic phases and one elastic phase. The six plastic phases can be reduced to just three considering that the plastic behaviour is symmetric. The force-displacement relationship for the elastic phases can be given by the following expression:

$$F_0^S(u) = F_I + k_0(u - u_I) \quad (5.2)$$

where (F_I, u_I) is the starting point of the elastic phase and k_0 its slope or the elastic stiffness of the spring. The three, in fact six, plastic phases are governed by the following equations:

$$F_J^S(u, \dot{u}) = F_J \text{sign}(\dot{u}) + h_J(u - u_J \text{sign}(\dot{u})); \quad (J = 1, 2, 3) \quad (5.3)$$

where (F_J, u_J) are characteristic points of the upper plastic phases. As it may be seen from Fig. 4.1(a), $u_2=0$, $h_1=h_3=k_2$ and $h_2=k_1$. The total number of parameters appearing in Eqn. 5.3 is equal to seven. An additional parameter, i.e. k_0 , is required for the definition of the elastic phases. However the following relationships hold among some of the parameters:

$$F_1 = F_2 + k_1 u_1; \quad F_3 = F_2 + k_1 u_3; \quad u_1 = -u_3 + 2 \frac{F_2}{(k_0 - k_1)} \quad (5.4)$$

Therefore five parameters are required to define the tri-linear model, namely F_2, u_3, k_0, k_1, k_2 . The bi-linear model can be obtained by setting $k_2=k_1$ and realising that u_3 is no longer needed. In this case the number of required parameters reduces to three, i.e. F_2, k_0, k_1 .

5.2. Constitutive behaviour of the friction slider

The constitutive behaviour of the friction slider is described by the equation:

$$F_F(u, \dot{u}) = (F_{F0} + k_F |u|) \text{sign}(\dot{u}) \quad (5.5)$$

At times when the system stops the friction force must satisfy the following inequality:

$$|F_F(u_R, 0)| \leq F_{F0} + k_F |u_R| \quad (5.6)$$

where u_R is the residual displacement.

6. ANALYTICAL SOLUTION

From the expressions of the restoring force in the tri-linear spring and of the friction force in the slider it follows that each phase of motion, either elastic or plastic, is governed by linear equations. Therefore, an analytical solution can be derived by standard methods for each phase of motion. Initial conditions in terms of displacement and velocity can be used to connect the solution of one phase of motion to that of the following one. As follows, the solutions to each of the four possible phases of motion will be

provided.

6.1. Elastic phases

The equation of motion for any elastic phase can be written as follows:

$$\ddot{u} + 2\zeta_0\omega_0\dot{u} + \tilde{\omega}_0^2u = \tilde{\omega}_0^2u_p \quad (6.1)$$

where the symbols have the following expressions:

$$\omega_0 = \sqrt{\frac{k_0}{m}}; \quad \zeta_0 = \frac{c}{2m\omega_0}; \quad \tilde{\omega}_0 = \rho_0\omega_0 \quad (6.2)$$

$$u_p = -\frac{(F_1 - k_0u_1 + F_{F0}\text{sign}(\dot{u}))}{k_0\rho_0^2}; \quad \rho_0 = \sqrt{1 + r_{F0}\text{sign}(u)\text{sign}(\dot{u})}; \quad r_{F0} = \frac{k_F}{k_0} \quad (6.3)$$

The solution to Eqn. 6.1 takes the simple form:

$$u(t) - u_p = u_a \exp\{-\zeta_0\omega_0(t - t_I)\} \cos[\tilde{\omega}_{0D}(t - t_I) - \theta_0] \quad (6.4)$$

where:

$$\sin\theta_0 = \frac{\dot{u}_I + (u_I - u_P)\zeta_0\omega_0}{u_a\tilde{\omega}_{0D}}; \quad \cos\theta_0 = \frac{u_I - u_P}{u_a} \quad (6.5)$$

$$\tilde{\omega}_{0D} = \omega_0\sqrt{\rho_0^2 - \zeta_0^2}; \quad u_a = \sqrt{(u_I - u_P)^2 + \left[\frac{\dot{u}_I + (u_I - u_P)\zeta_0\omega_0}{\tilde{\omega}_{0D}}\right]^2} \quad (6.6)$$

In the expressions above u_I and \dot{u}_I are the initial conditions for the considered elastic phase. It should be noticed that when the elastic phase starts from the end of a plastic one it is $\dot{u}_I=0$, from which it follows that $\theta_I=\theta_0$. Velocity and acceleration take similar expressions:

$$\dot{u}(t) = -\dot{u}_a \exp\{-\zeta_0\omega_0(t - t_I)\} \sin[\tilde{\omega}_{0D}(t - t_I) - \theta_0 + \theta_1] \quad (6.7)$$

$$\ddot{u}(t) = -\ddot{u}_a \exp\{-\zeta_0\omega_0(t - t_I)\} \cos[\tilde{\omega}_{0D}(t - t_I) - \theta_0 + 2\theta_1] \quad (6.8)$$

where:

$$\sin\theta_1 = \frac{\zeta_0}{\rho_0}; \quad \cos\theta_1 = \frac{\sqrt{\rho_0^2 - \zeta_0^2}}{\rho_0}; \quad \dot{u}_a = \tilde{\omega}_0u_a; \quad \ddot{u}_a = \tilde{\omega}_0\dot{u}_a = \tilde{\omega}_0^2u_a \quad (6.9)$$

6.2. Plastic phases

The equation of motion for any of the plastic phases takes the following expression:

$$\ddot{u} + 2\zeta_J\omega_J\dot{u} + \tilde{\omega}_J^2u = \tilde{\omega}_J^2u_J^p \quad (6.10)$$

where:

$$\omega_J = \sqrt{\frac{h_J}{m}}; \quad \zeta_J = \frac{c}{2m\omega_J}; \quad \tilde{\omega}_J = \rho_J \omega_J; \quad (J=1,2,3) \quad (6.11)$$

$$u_J^p = -\frac{(F_J - h_J u_J + F_{F0}) \text{sign}(\dot{u})}{h_J \rho_J^2}; \quad (J=1,2,3) \quad (6.12)$$

$$\rho_J = \sqrt{1 + r_{FJ} \text{sign}(u) \text{sign}(\dot{u})}; \quad r_{FJ} = \frac{k_F}{h_J}; \quad (J=1,2,3) \quad (6.13)$$

The solution to the equation of motion is given below in terms of displacement, velocity and acceleration:

$$u(t) - u_J^p = u_J^a \exp\{-\zeta_J \omega_J (t - t_I)\} \cos[\tilde{\omega}_{JD} (t - t_I) - \Theta_J] \quad (6.14)$$

$$\dot{u}(t) = -\dot{u}_J^a \exp\{-\zeta_J \omega_J (t - t_I)\} \sin[\tilde{\omega}_{JD} (t - t_I) - \Theta_J + \Phi_J] \quad (6.15)$$

$$\ddot{u}(t) = -\ddot{u}_J^a \exp\{-\zeta_J \omega_J (t - t_I)\} \cos[\tilde{\omega}_{JD} (t - t_I) - \Theta_J + 2\Phi_J] \quad (6.16)$$

where:

$$\tan \Theta_J = \frac{\dot{u}_I + (u_I - u_J^p) \zeta_J \omega_J}{(u_I - u_J^p) \tilde{\omega}_{JD}}; \quad \tan \Phi_J = \frac{\zeta_J}{\sqrt{\rho_J^2 - \zeta_J^2}}; \quad \tilde{\omega}_{JD} = \omega_J \sqrt{\rho_J^2 - \zeta_J^2} \quad (6.17)$$

$$u_J^a = \sqrt{(u_I - u_J^p)^2 + \left[\frac{\dot{u}_I + (u_I - u_J^p) \zeta_J \omega_J}{\tilde{\omega}_{JD}} \right]^2}; \quad \dot{u}_J^a = \tilde{\omega}_J u_J^a; \quad \ddot{u}_J^a = \tilde{\omega}_J \dot{u}_J^a = \tilde{\omega}_J^2 u_J^a \quad (6.18)$$

7. NUMERICAL APPLICATION

The following numerical application is meant to demonstrate the derived analytical solution. The simulation of Test 5 on the Solarino building is performed using as model parameters the best identified ones. The only purpose of this section is to illustrate the solution, while the identification problem is dealt within a following section. The solution is provided in terms of displacement, velocity and acceleration, as well as in terms of the force-displacement relationship for the HDRB and LFSB components of the HIBS isolation system. The results are shown in Fig. 7.1. In Fig. 7.1(a) the simulated acceleration is compared to the experimental record, while in Fig. 7.1(b) the simulated acceleration graph is partitioned according to the successive elastic and plastic phases of motion. The continuous branches are separated by acceleration jumps due to changes of sign in the friction force. Altogether there are three cycles of motion before the system comes to rest, each one composed of two branches. In the first branch, the elastic phase is followed by plastic phases 1 and 2. The second, third and fourth branch show elastic phases alternating only with plastic phase 2. The last cycle is formed by two fully elastic branches. Fig. 7.1(c) and Fig. 7.1(d) show the time-displacement and the time-velocity graphs respectively. A residual displacement of 3 mm in the displacement graph and a maximum velocity of the order of 26 cm/s in the velocity graph should be noticed. The six branches of elastic behaviour can be clearly seen also in Fig. 7.1(e), where the force-displacement graph for the HDRB component of the isolation system is shown. It should be noticed that the identification of the experimental data has provided the following inequalities between the slopes of the force-displacement relationship: $k_0 > k_1 > k_2$. This property will be discussed, along with others, in the identification section of the paper. Finally, Fig. 7.1(f) shows the force-displacement relationship for the LFSB component. It may be worth noticing that the identification procedure provided a friction force-displacement relationship where the friction force increases, albeit slightly, with the displacement amplitude.

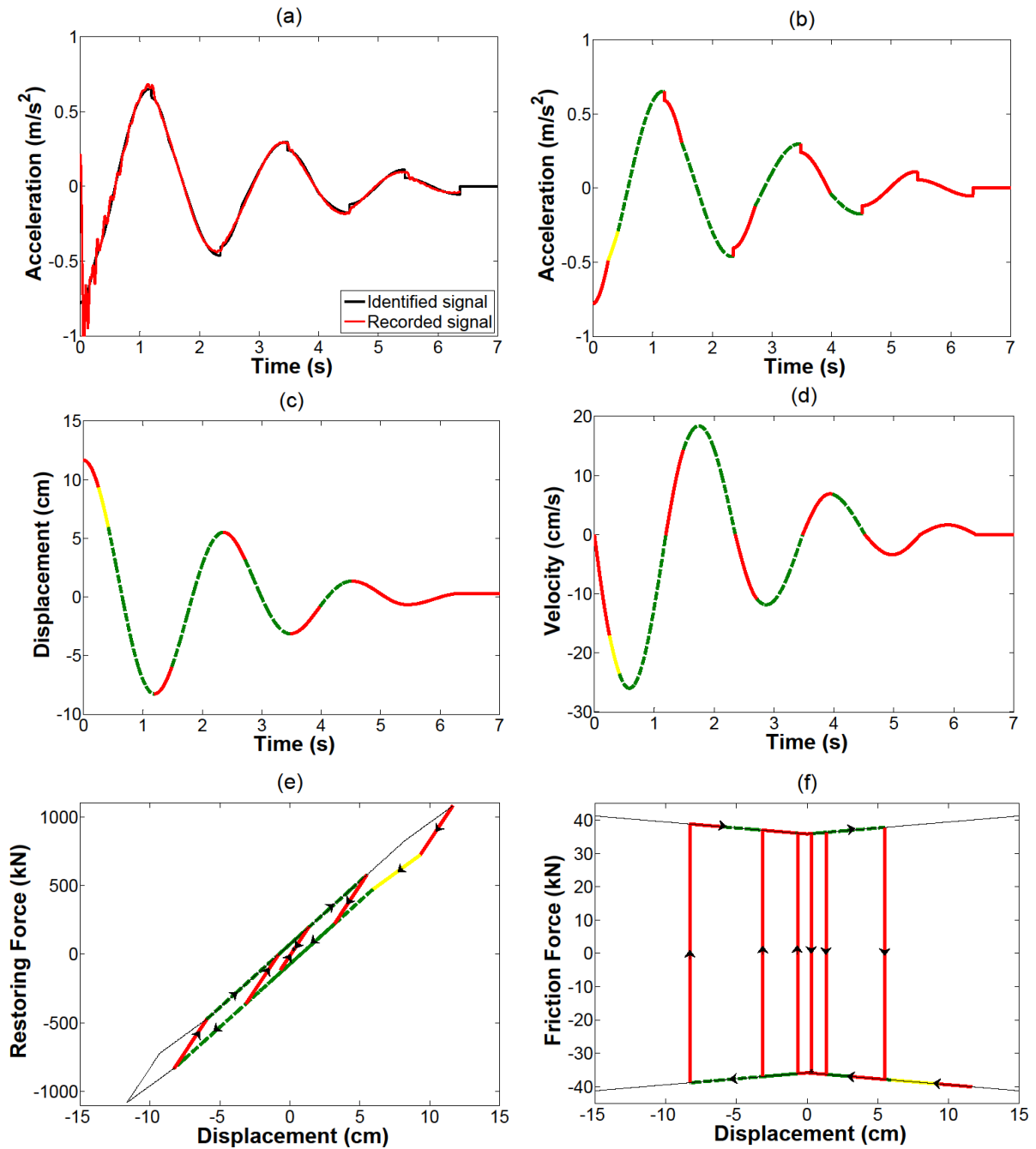


Figure 7.1. (a) Identified and recorded acceleration, (b) acceleration-time, (c) displacement-time, (d) velocity-time, (e) restoring force-displacement, (f) friction force-displacement

8. THE IDENTIFICATION PROBLEM

The Solarino free vibration tests were performed with the goal of identifying the system parameters from the recorded acceleration response. A displacement of the order of magnitude of the design one was initially imposed to the building and the corresponding force suddenly released. The testing apparatus and the data acquisition system used in the tests are described in (Oliveto et al., 2004(b)). Identification procedures in the frequency domain, using equivalent viscous models, proved to be unsuitable since they were unable to predict the clear shortening of the period with the decay of amplitude. The constant period of the viscous equivalent model was in stark contrast with the experimental data, (Oliveto et al., 2008). For this reason, a more sophisticated model was introduced for

identification in the time domain, including a bi-linear spring to model the HDRB, a Coulomb friction slider to model the LFSB and a viscous damper to account for damping in the superstructure. An analytical solution for such a model was derived in (Oliveto et al., 2010) and applied to the system identification in the time domain using an iterative least squares procedure. The results were good, but the identification procedure was interactive, required considerable expertise and was time consuming. The authors concluded that there was still ample space for improvement, both in terms of modelling and identification procedure. The improvement of the identification procedure involved the establishment of bounds for the system parameters and the use of the CMA-ES algorithm. These two expedients made the identification procedure completely automatic and much faster. The CMA-ES was the most successful evolution strategy among the ones applied to the present problem, as documented in the interdisciplinary literature, (Athanasiou et al., 2011 and 2012). As far as modelling is concerned enhancements were originally achieved by introducing a two parameter model for the friction slider (LCFM), (Athanasiou and Oliveto, 2011). This course of action was motivated by the experimental observation that the friction force appears to be larger when the amplitude of motion is higher. In the present work the sign of the slope of the LCFM has been left free, so that the identification procedure can select positive or negative values according to what is required by the optimization process. The most noticeable improvement of the present work has been the introduction of the tri-linear spring to model the HDRB. The analytical solution provided in section 6 has allowed for a simple calculation of the error of the trial solution, i.e. the distance between the trial solution and the experimental one. The same approach proposed in (Oliveto et al., 2010) has been used for the evaluation of the error, or “solution fitness” in evolutionary computation jargon. Before moving to illustrate the results, it may be worth noticing that the CMA-ES algorithm is readily available, well documented and still subject of active research aiming at establishing its full potential and limits, (Hansen et al., 2011).

8.1. Identification results

The best results obtained by the identification procedure, using the most advanced model described in the previous section, are shown in Table 8.1. The identified system parameters are listed in the first column. Each quantity considered corresponds to a model parameter introduced in previous sections. In the first row is the “nominal” imposed displacement for each of the five dynamic tests considered. In the second row is the identified initial displacement u_0 ; in the third is the first yield displacement u_y , related to the force F_2 and to the stiffness coefficients k_0 and k_1 by the relationship $u_y = F_2 / (k_0 - k_1)$, see Fig. 4.1(a). In the fourth row is the friction displacement defined as $u_{F0} = F_{F0} / k_0$, see Fig. 4.1(a) and (b), while in the fifth and sixth rows are the stiffness ratio r_{F0} , defined by Eqn. 6.3, and the damping ratio ζ_0 , defined by Eqn. 6.2. In rows seven, eight and nine are three frequency parameters f_0 , f_1 and f_2 , specified in cycles per second, corresponding to the circular frequencies defined by Eqn. 6.2 and 6.11. These are the characteristic frequencies of the system determining the change of period with amplitude. In the tenth row is the second yield displacement u_3 , Fig. 4.1(a), while in the eleventh row a measure of the identification error is given, see (Oliveto et al., 2010) for the definition. The last two columns provide for each system parameter the average value obtained from the five tests considered and the coefficient of variation. It is easy to recognize that the most stable parameters, i.e. those with the smallest variation from test to test, are the characteristic frequencies f_0 and f_1 , followed by the friction displacement u_{F0} , the characteristic frequency f_2 , the two yield displacements u_y and u_3 , and the damping ratio ζ_0 . The most uncertain parameter appears to be the slope of the friction force – displacement graph. Of the five tests considered only one shows an increasing friction force with the displacement amplitude, Fig. 7.1(f), while all the others show a behavior consistent with Fig. 4.1(b). A consistent comparison with results from previous models may be found in (Athanasiou et al., 2011 and 2012).

8.2. Identified physical parameters

Using the identified mathematical parameters, the significant physical quantities of the system have been evaluated using the method outlined in (Oliveto et al., 2010). The results are shown in Table 8.2. The main aspect that emerges from the use of the new model is an increase of the stiffness coefficients k_0 and

k_l with respect to those obtained with the bi-linear model, (Oliveto et al., 2010), and a corresponding decrease of the first yield displacement u_y .

Table 8.1. Results from the identified five dynamic tests of Solarino.

Test	3	5	6	7	8	Mean	c.o.v. (%)
u_0 n. (m)	0.11480	0.13290	0.13080	0.09670	0.10750	-	-
u_0 (m)	0.10753	0.11660	0.11391	0.08500	0.08999	-	-
u_y (m)	0.00898	0.01167	0.01069	0.00848	0.00732	0.00943	17
u_{F_0} (m)	0.00179	0.00234	0.00217	0.00218	0.00245	0.00219	10
r_{F_0}	-0.00119	0.00235	-0.00706	-0.01466	-0.02912	-0.00994	-113
ζ_0	0.02962	0.02256	0.02149	0.03583	0.04461	0.03082	28
f_0 (Hz)	0.56318	0.53979	0.56118	0.55743	0.55218	0.55475	2
f_1 (Hz)	0.43089	0.41723	0.42171	0.44264	0.44805	0.43210	3
f_2 (Hz)	0.26401	0.37477	0.30483	0.32331	0.29516	0.31242	12
u_3 (m)	0.06951	0.08252	0.07611	0.05358	0.05696	0.06773	16
e^2	0.00489	0.00431	0.00538	0.00655	0.00305	-	-

Table 8.2. Physical quantities from the identified five dynamic tests of Solarino.

Test	m (tn)	k_0 (kN/m)	k_1 (kN/m)	k_2 (kN/m)	k_F (kN/m)	c (kNs/m)	F_0^n (kN)	F_0 (kN)	F_{fs}^a (kN)
3	1438	18004	10539	3957	-21	301	1050	1027	77
5	1333	15332	9160	7390	36	204	1180	1140	60
6	1535	19089	10780	5632	-135	233	1222	1177	55
7	1319	16183	10204	5444	-237	331	868	828	60
8	1457	17537	11546	5011	-511	451	967	927	60
Mean	1416	17229	10446	5487	-174	304	-	-	-
c.o.v. (%)	6	8	7	20	-111	28	-	-	-

Contrary to expectations, the third stiffness coefficient k_2 is always smaller than both k_0 and k_1 , giving the impression that the force-displacement relationship for the HDRB exhibits a gradually decreasing slope as the displacement amplitude increases. This softening effect may be due to the combined action of vertical load and large horizontal displacements. The damping ratio ζ_0 , which is probably related to damping in the superstructure, is on average equal to 0.03, with a minimum value slightly above 0.02 and a maximum value of about 0.045. The evaluated system mass is on average about 18% larger than in previous calculations. As explained in (Oliveto et al., 2010), the evaluation has been performed using the formula given below and slightly modified to account for the tri-linear model introduced herein:

$$m = \frac{F_0^n - F_{fs}^a}{\omega_0^2 u_y + \omega_1^2 (u_3 - u_y) + \omega_2^2 (u_0 - u_3)}; \quad F_0^n = F_0 + (F_{fs} - F_{fs}^a) \quad (8.1)$$

The change consists of reassessing the released force to account for the force entrapped in the system due to residual displacements (forces in the HDRB balancing those in the LFSB). The new values of the released force are given in the column under F_0^n in Table 8.2. The correction term is due to the difference between the friction force evaluated during the first static test F_{fs} (not affected by residual displacements) and the apparent friction force F_{fs}^a measured in the static pushing phases before the dynamic release tests (affected by residual displacements), (Oliveto et al., 2004(b)). The value of the static friction force F_{fs} used in the above calculations is 100 kN, corresponding to the lower value of the two considered in the quoted references.

9. CONCLUSIONS

A new model for the simulation of the free vibration response of HBIS, composed of HDRB and LFSB, has been presented. It has been shown that the non-linear behaviour of the model derives from alternating phases of different linear behaviours. This ensures the existence of an analytical solution, which has been derived for the case of release tests under imposed initial displacement. This solution has been used, in conjunction with a state-of-the-art algorithm based on evolution strategies, for the identification of the HBIS of the Solarino buildings. A better matching of the simulated and the experimental responses has been achieved than that obtained using previous models. Particularly relevant has been the discovery that the slope of the force-displacement relationship for the HDRB component of the HBIS is monotonically decreasing with the increase of the displacement amplitude, i.e. $0 < k_2 < k_1 < k_0$. However, it is always positive for the displacements considered in the tests. Viscous damping, accounting for energy dissipation in the superstructure, also contributes to an improvement of the identification results, as compared to those obtained when it is neglected.

ACKNOWLEDGEMENT

This work has been carried out within the PRIN 2007 project "Seismic Retrofitting of Buildings using Isolation and/or Energy Dissipation Techniques: Design, Modelling, Identification". The first (AAM) and second (AA) authors were supported by scholarships under PRIN 2007 and EU FSE funds.

REFERENCES

- Oliveto, G., Calio, I. and Marletta, M. (2004(a)). Retrofitting of Reinforced Concrete Buildings not Designed to Withstand Seismic Action: a Case Study Using Base Isolation. *13th World Conference on Earthquake Engineering*. Vancouver, Canada, 954-968.
- Oliveto, G., Granata, M., Buda, G. and Sciacca, P. (2004(b)). Preliminary Results From Full-Scale Free Vibration Tests on a Four Story Reinforced Concrete Building after Seismic Rehabilitation by Base Isolation. *JSSI 10th Anniversary Symposium on Performance of Response Controlled Buildings*. Yokohama, Japan, 126-135.
- Oliveto, N.D., Scalia, G. and Oliveto, G. (2008). Dynamic identification of structural systems with viscous and friction damping. *Journal of Sound and Vibration* **318:6**, 911–926.
- Oliveto, N.D., Scalia, G. and Oliveto, G. (2010). Time domain identification of hybrid base isolation systems using free vibration tests. *Earthquake Engineering and Structural Dynamics* **39:9**, 1015-1038.
- Athanasίου, A. and Oliveto, G. (2011). Modelling Hybrid Base Isolation Systems for Free Vibration Simulations. *8th International Conference on Urban Earthquake Engineering*. Tokyo, Japan, 1293-1302.
- Athanasίου, A., De Felice, M., Oliveto, G. and Oliveto, P.S. (2011). Evolutionary Algorithms for the Identification of Structural Systems in Earthquake Engineering. *In Proceedings of the International Conference on Evolutionary Computation Theory and Applications (ECTA'11)*, 52-62.
- Athanasίου, A., De Felice, M., Oliveto, G. and Oliveto, P.S. (2012). Dynamical Modeling and Parameter Identification of Seismic Isolation Systems by Evolution Strategies, *Studies in Computational Intelligence*, Springer-Verlag.
- Hansen, N. (2006). The CMA evolution strategy: a comparing review. In: J. Lozano, P. Larranaga, I. Inza, E. Bengoetxea (Eds.), *Towards a new evolutionary computation*. Advances on estimation of distribution algorithms. *Springer*, 75–102.
- Constantinou, M.C., Whittaker, A.S., Kalpakidis, Y., Fenz, D.M., and Warn, G.P. (2007). Performance of Seismic Isolation Hardware under Service and Seismic Loading. Technical Report MCEER
- Kasai, K. (2009). Special Issue on "Japan's Advanced Technology for Building Seismic Protection". *Journal of Disaster Research* **4:3**.
- Wada A., and Constantinou, M. C. (2010). Special EESD Issue on Seismic Protection Techniques. *Earthquake Engineering and Structural Dynamics* **39:13**.
- Hansen, N., Ros, R., Mauny, N., Schoenauer, M. and Auger, A. (2011). Impacts of Invariance in Search: When CMA-ES and PSO Face Ill-Conditioned and Non-Separable Problems.. *Applied Soft Computing* **11**, 5755-5769.